Published in final edited form as:
J Magn Reson Imaging. 2012 August ; 36(2): 430–437. doi:10.1002/jmri.23672.

Multiparametric 3-Tesla Endorectal MR Imaging after External Beam Radiation Therapy of Prostate Cancer

Antonio C. Westphalen, MD[1], **Galen D. Reed, BS**[1], **Phillip P. Vinh, DO**[1], **Christopher Sotto, BS**[1], **Daniel B. Vigneron, PhD**[1], and **John Kurhanewicz, PhD**[1]

[1]Department of Radiology and Biomedical Imaging, University of California, San Francisco

Abstract

Purpose—To determine the best combination of magnetic resonance (MR) imaging parameters for the detection of locally recurrent prostate cancer after external beam radiation therapy.

Materials and Methods—Our IRB approved this study with a waiver of informed consent. Twenty-six patients with suspected recurrence due to biochemical failure were part of this research. The MR protocol included T2-weighted, MR spectroscopic, and diffusion-weighted MR imaging. Transrectal ultrasound-guided biopsy was the standard of reference. We used logistic regression to model the probability of a positive outcome and generalized estimating equations to account for clustering. The diagnostic performance of imaging was described using receiver operating characteristic (ROC) curves.

Results—The area under the ROC curve of MR spectroscopic imaging (MRSI) was 83.0% (95% CI = 75.5 to 89.1). The combination of all MR techniques did not significantly improve the performance of imaging beyond the accuracy of MRSI alone, but a trend towards improved discrimination was noted (86.9%; 95% CI = 77.6 to 93.4; $P = 0.09$).

Conclusion—In conclusion, incorporation of MRSI to T2-weighted and/or diffusion-weighted MR imaging significantly improves the assessment of patients with suspected recurrence after radiotherapy and a combined approach with all three modalities may have the best diagnostic performance.

Keywords

MRI; MR spectroscopy; diffusion MRI; prostate cancer; radiation therapy

INTRODUCTION

Over 240,000 new cases of prostate cancer will be diagnosed in 2011 (1) and many will be treated with external beam radiation therapy (2). Approximately half of these patients are expected to develop biochemical failure, i.e. a rising serum prostatic specific antigen (PSA) after a post-treatment nadir has been reached (3,4), which triggers investigation for local and/or systemic disease. Despite being an invasive method fraught with sampling error, the diagnosis or exclusion of locally recurrent cancer is routinely performed by TRUS biopsy (5,6).

Endorectal magnetic resonance (MR) imaging may assist in overcoming this problem; it allows for the identification of the whole gland and imaging findings can potentially be used

Corresponding author Antonio C. Westphalen, MD., 505 Parnassus Avenue, Box 0628, M-372, San Francisco, CA 94143-0628, Tel: (415) 353-1945 Fax: (415) 476-0616, antonio.westphalen@ucsf.edu.

to target only suspicious areas. Yet, T2-weighted MR imaging also has limitations in the post-radiation setting related to radiation-induced atrophy and fibrosis (7,8). Functional and metabolic MR sequences provide information that is incremental to that obtained with anatomical T2-weighted MR images. While a few prior studies have investigated the benefit of these sequences when compared to T2-weighted MR imaging (9–12), it is unclear if the combination of more than one of these techniques improves the detection of recurrent cancer. In addition, 3-Tesla magnets that were once exclusively seen in academic centers are now widely available. Images acquired using these magnets have higher spatial and/or temporal resolution than images acquired on 1.5-Tesla magnets; but at the same time these studies are more susceptible to artifacts that may degrade the quality of images and reduce its interpretability (13).

Anecdotally, we have noticed in our practice that ADC values of post-radiation atrophic tissue and locally recurrent prostate cancer measured on 3-Tesla scanners using endorectal coil differ from ADC values seen in untreated gland and untreated tumor. Song et al. in a recent study suggested that ADC values of noncancerous areas of the prostate decrease following radiation therapy, but did not describe the actual ADC values (14). Also, in their study patients were scanned using only a pelvic phased-array coil.

Accordingly, the goals of this study were to compare the diagnostic performance of 3-Tesla T2-weighted MR imaging, MR spectroscopic imaging, and diffusion-weighted MR imaging, determining the best combination for the detection of recurrent prostate cancer after external beam radiation therapy, and, secondarily, to describe the ADC values of atrophic prostatic tissue and recurrent prostate cancer.

MATERIALS AND METHODS

Subjects

This retrospective single institution study was approved by our Committee on Human Research with a waiver of informed consent and was compliant with requirements of the Health Insurance Portability and Accountability Act.

We retrospectively identified all patients who met the following inclusion criteria:

1. Patients with biopsy-proven prostate cancer treated with primary external beam radiation therapy (with or without associated androgen deprivation therapy).
2. Post-treatment 3-Tesla endorectal MR imaging of the prostate performed between January 2007 and March 2010 for assessment of suspected local recurrence due to biochemical failure, based on three consecutive rises of PSA or a rise by 2 ng/mL or more above the nadir PSA, as recommended by the American Society for Therapeutic Radiology and Oncology (15).
3. Post-treatment transrectal ultrasound-guided biopsy of the prostate.
4. No post-radiation salvage treatment (e.g. salvage brachytherapy or salvage prostatectomy) administered prior to MR imaging or biopsy.

Twenty-six patients with mean age of 69 years (range, 54 to 78) fulfilled these criteria. There were no exclusion criteria. One author (PPV) reviewed all medical and clinical records to collect all available pre- and post-treatment and histopathological data.

Imaging Acquisition

All studies were performed on a GE 3.0 Tesla scanner (GE Healthcare Technologies, Waukesha, WI) using body coil for excitation and a Medrad inflatable endorectal coil

(Medrad, Pittsburgh, PA) filled with perfluorocarbon (3M, Saint Louis, MO) in conjunction with a pelvic phase array coil for signal reception. After a localizer image, the following MR sequences were obtained:

- Axial spin-echo T1-weighted images from the aortic bifurcation to the symphysis pubis. TR/TE = 600–700/12 msec. Slice thickness = 4–6 mm. Interslice gap = 0–1 mm. Matrix 256 × 192. Frequency direction transverse (to prevent obscuration of pelvic nodes by endorectal coil motion artifact). Number of excitations = 1. Field of view = 20–32 cm. Acquisition time = 2–3 mins.
- Thin-section high-resolution oblique axial and coronal T2-weighted fast spin-echo images of the prostate and seminal vesicles (planes were selected relative to the long axis of the prostate). TR/TE = 4000–6000/90–120 msec. Echo train length = 8–16. Slice thickness = 3 mm. Interslice gap 0 mm. Matrix 256 × 192. Frequency direction anteroposterior (to prevent obscuration of the prostate by endorectal coil motion artifact). Number of excitations = 3. Field of view = 14 cm. Acquisition time = 2 to 8 mins.
- 3D MRSI data were acquired with MLEV-PRESS sequence (16) that allows the acquisition of completely upright citrate resonance at TE of 85ms with a 0.157cc nominal spatial resolution. The MRSI parameters were as follows: TR = 2.0 s; TE = 85ms; NEX = 1; phase encoding steps = 16 × 10 × 8; FOV = 86 × 54 × 43 mm^3; scan time = 11 min. An interleaved echo-planar spectroscopic readout was used in the left-right dimension.
- Oblique axial DTI-EPI images with 6 diffusion gradient directions were acquired in 2.5 minutes with a FOV = 24 cm, 256 × 128 matrix, 4mm thick slices, and b-value of 600 s/mm^2, with 8–10 slices typically to cover the prostate. For prostate diffusion-weighted MR imaging studies, investigators have used multiple B-values ranging from 0–1000 s/mm^2. For those using 0 s/mm^2 and another b-value, investigators have typically used 500 to 800 s/mm^2 as their second b-value (17–19). We found 0 s/mm^2 and 600 s/mm^2 provided good ADC contrast to noise in the prostate. At high b-values (1,000 to 2,000 s/mm^2), images are very sensitized to motion and there is a corresponding dramatic drop in signal-to-noise ratio.

Diagnostic Performance: Imaging Interpretation

T2-weighted MR imaging—A single radiologist (ACW, 7 years of experience in genitourinary imaging) reviewed all MR images on a picture archiving and communication system workstation (Impax; Agfa, Mortsel, Belgium), and rated recurrent tumor as present or absent in each sextant of the prostate. A sextant was defined as one of the following divisions of the prostate: right base, right middle gland, right apex, left base, left middle gland, and left apex. Right and left sides were determined by an imaginary line coursing through the center of the gland, from anterior to posterior on the axial plane, dividing the prostate in two halves. There are no structural landmarks that delineate the margins between the base, middle gland, and apex of the prostate. Accordingly, these locations on oblique axial T2-weighted images were determined through cross-referencing with coronal images. Tumor was considered present if a mass-like nodule was seen in the prostate or if a crescentic subcapsular focus of low T2 signal intensity was seen in the peripheral zone. The reader was aware that these patients had an elevated PSA following radiation therapy, but did not have access to any other clinical or laboratorial information, including prior imaging studies and serum PSA level.

Diffusion-weighted MR imaging—The radiologist who interpreted the T2-weighted images also reviewed all diffusion-weighted MR images. This was done in a separate session, without access to the T2-weighted MR images, 8 weeks later. These data were assessed using apparent diffusion coefficient (ADC) maps. No threshold was applied to these calculated maps. The reader drew regions of interest (ROI) on all suspicious foci seen on the ADC maps and ADC values were recorded. A suspicious focus was defined as an area of low signal intensity on visual inspection, based on the knowledge that prostate cancer has lower ADC values than normal prostatic tissue (20). The sextant in which an abnormal finding was seen was determined based on the side of the gland and on the number of images obtained. The total number of images was divided by three. The apex was defined as the images representing the most caudal third of the gland, followed by the middle gland and then base. If the total number of images did not allow for an even division, the first extra slice was considered to represent the middle gland, and next one, the apex.

MR spectroscopic imaging—One of the authors (JK, 20 years of experience) evaluated the spectra after baseline correction and automated frequency shifting to optimize the alignment of statistically significant peaks (signal-to-noise ratio, >5:1) in the spectrum with the expected locations of choline, creatine, citrate, and residual water resonances. Subsequently, a zero-order phase was applied to generate an upright and symmetric water resonance, and metabolite resonances were baseline corrected by using local nonlinear fitting to the nonpeak regions of the spectra. After evaluation of quality of each MR spectroscopic study, spectra were analyzed with a quantification algorithm that provides estimates of metabolite peak areas and random noise. Metabolite peak areas were obtained by numeric integration of the in-phase component of the spectra over frequency regions corresponding to choline and creatine. Spectra were summed over a 29.6 Hz bandwidth for choline (30 points) and over a 19.8 Hz width for creatine (20 points). These values were normalized by the standard deviation of a 138 Hz region (140 points) devoid of metabolite signal centered 188 Hz higher than the water resonance.

Previous research has shown that following radiation therapy the levels of citrate and polyamines are dramatically reduced on MR spectroscopic imaging and that successful treatment is characterized by a lack of metabolic activity or “metabolic atrophy” (21–23). However, residual or recurrent prostate cancer can be detected by identification of choline or of a relative increase in the choline/creatine ratio (12). To avoid divergent values, choline-to-creatine ratios were calculated only on voxels in which both resonances had SNR values of at least 5. Voxels were considered unremarkable if no metabolism was identified or if the spectrum showed a choline-to-creatine less than 1.5. A choline-to-creatine ratio greater than 1.5 or identification of choline in the absence of creatine was considered abnormal. Identification of three consecutive abnormal voxels within a sextant, either in-plane or through-plane, characterized a positive result on MR spectroscopic imaging (12). T2-weighted images with an MR spectroscopic overlay were available to the reader to allow for localization of findings into sextants.

Standard of Reference

Transrectal ultrasound-guided biopsy was the standard of reference in this study. All but two biopsies were performed at our institution. The usual number of specimens that were obtained was 16, using a systematic approach that targeted the right and left sides of the gland at different levels, as well as suspicious areas seen on ultrasound. Samples processed at our institution were fixed in formalin immediately after biopsy and subsequently placed in a block of paraffin wax. Microtome sections were then mounted on a glass slide and stained with hematoxylin and eosin. High molecular weight keratin immunoperoxidase staining was also performed on areas suspicious for adenocarcinoma. Histopathological evidence of post-

treatment effect only, i.e. associated with negative immunoperoxidase staining, was considered a negative result (24,25). The presence of cancer on all histopathology reports was recorded on a per-sextant basis. One author (PPV) retrospectively reviewed these reports to determine the presence or absence of cancer within each sextant of the prostate.

Statistical Analysis

The prostate sextant was used as the unit of analysis in this study. The study sample data was described using median and interquartile range. We used logistic regression with A) a single predictor (T2-weighted MR imaging results, diffusion-weighted MR imaging results, or MR spectroscopic imaging results), B) two predictors (T2-weighted MR imaging and MR spectroscopic imaging results, T2-weighted MR imaging and diffusion-weighted MR imaging results, or MR spectroscopic imaging and diffusion-weighted MR imaging results) and C) three predictors (T2-weighted MR imaging results, diffusion-weighted MR imaging results, and MR spectroscopic imaging results) to model the probability of a positive outcome. The models were built without any other pre-specified conditions for the inclusion of these parameters. We used generalized estimating equations to take into account the clustering effect related to the artificial division of the prostate (sextants) (26). The performance of each diagnostic approach was described using receiver operating characteristic curves. We used cluster resampled, bias-corrected, bootstrap confidence intervals to compare the differences between the areas under the receiver operating characteristic curves (27).

We used the Wilcoxon rank-sum test to compare the mean ADC values of atrophic prostatic tissue and recurrent prostate cancer.

Statistical calculations were performed using Stata 11.2 (College Station, TX). All test were two-tailed and a 5% level of confidence was considered to be significant.

RESULTS

Patient population

The median pre-treatment PSA and Gleason sum at the time of prostate cancer diagnosis were 10.1 ng/ml (interquartile range or IQR = 5.4 to 14.0) and 7 (IQR = 6 to 7), respectively. All but three (23/26) patients had localized disease based on clinical staging.

Patients received a median radiation dose of 72 Gy (IQR = 72 to 75); nineteen men were also treated with neoadjuvant androgen deprivation therapy. The median post-treatment PSA nadir was 0.3 ng/ml (IQR = 0.1 to 0.8).

The median PSA level at the time of imaging was 2.5 ng/ml (IQR = 1.6 to 3.2). The median time interval between biopsy and imaging was 16 days (IQR = 5 to 34), with only 3 patients having an interval greater than 34 days.

Recurrent prostate cancer was identified by biopsy in 14 of 26 patients (53.8%), and was unilateral in 9 and bilateral in 5 (for total of 35 affected sextants).

The median time between end of treatment and imaging was 164 months (IQR = 119.6 to 199.2).

MR Imaging

One hundred and eleven of 121 sextants without evidence of recurrent cancer on biopsy had no suspicious areas of T2-weighted MR imaging. Only eleven of 35 sextants with positive biopsies had an abnormal area of low signal intensity.

One hundred and four of 121 negative sextants on biopsy presented with atrophic metabolism on MR spectroscopic imaging. Conversely, twenty-eight of 35 positive sextants had abnormal metabolism.

One hundred and ten of 121 sextants without evidence of cancer on biopsy had negative findings on diffusion-weighted MR imaging. Twenty of 35 patients with biopsy-proven recurrent cancer had true-positive results. The mean ADC value of biopsy-negative regions was 1.6×10^{-3} mm^2/s (standard deviation or SD = 0.2), significantly higher than the average value seen in foci of recurrent cancer (1.0×10^{-3} mm^2/s, SD = 0.1; $P < 0.001$).

Only five sextants in 5 patients were found to have cancer in spite of all three modalities being negative; in 2 of these patients MR imaging identified other sextants with disease.

Receiver-operating characteristic curves—The area under the receiver operating characteristic (ROC) curve of diffusion-weighted MR imaging by itself (75.5%; 95 % CI = 61.0 to 85.3) was not statistically different from that of T2 weighted imaging (61.6%; 95% CI = 51.1 to 73.2; $P = 0.07$) or MR spectroscopic imaging (83.0%; 95% CI = 75.5 to 89.1; $P = 0.20$) alone. However, MR spectroscopic imaging performed significantly better than T2-weighted imaging alone ($P = 0.001$).

T2-weighted MR imaging alone performed worse than any combination of MR techniques, and applying it with diffusion-weighted MR imaging and/or MR spectroscopic imaging did not improve the discrimination between positive and negative sextants.

The combination of MR spectroscopic imaging with diffusion-weighted MR imaging (86.3%; 95% CI = 77.5 to 93.3) was more accurate than diffusion-weighted MR imaging alone ($P = 0.02$).

The areas under the ROC curves for the combination of any two or all three MR techniques were not larger than that of MR spectroscopic imaging alone. These results are summarized in tables 1 and 2. Figure 1 depicts the ROC curves of MR spectroscopic imaging alone, MR spectroscopic imaging and diffusion-weighted MR imaging, and all three MR modalities, and an illustrative case is shown in figure 2.

DISCUSSION

The results of this study suggest that multiparametric MR imaging is a good tool for assessing patients with suspected locally recurrent cancer after radiation therapy; in particular, concordant negative results exclude disease in the majority of patients.

The performance of T2-weighted imaging alone was poor and when this parameter was combined with diffusion-weighted MR imaging and/or MR spectroscopic imaging the area under the ROC curves did not change significantly. As shown before (28), these results suggest that T2-weighted MR imaging cannot be used individually to assess patients with suspected locally recurrent prostate cancer after external beam radiation therapy; yet it likely has a role in anatomical localization.

Individually, the performance of diffusion-weighted MR imaging and MR spectroscopic imaging were not significantly different (p-value of 0.20); however, the combination of both modalities had higher discrimination power when compared to diffusion-weighted MR imaging alone, but not MR spectroscopic imaging.

Even though MR spectroscopic imaging appears to achieve good results by itself, the combination of three modalities led to better results. Although the difference between the

areas under the ROC curves was not statistically significant ($P = 0.09$), analysis of the ROC curves shapes demonstrate that all three modalities together are more sensitive for the detection of recurrent cancer. The specificity of MR imaging, however, does not change to an appreciable extent. These findings suggest that that diffusion-weighted MR imaging, and to a lesser extent T2-weighted MR imaging, is important components of multiparametric MR scans of the prostate of patients treated with external beam radiation therapy. It is also important to remember that adequate acquisition of spectroscopic data is dependent on the expertise available. Some centers have dedicated spectroscopists who perform both pre and post processing of data and manual case-by-case adjustments that result in significantly better spectra than commercially available software. However, most centers do not have the benefit of such dedicated personnel. The acquisition and quality of diffusion-weighted MR imaging, though, tends to be more homogeneous throughout different platforms and institutions.

The acquisition time of diffusion-weighted MR images is short and does not significantly interfere with the total scanning time. Furthermore, with the recent FDA approval of perfluorocarbon, an inert liquid with similar magnetic susceptibility to that of the prostate, for use with 3-Tesla endorectal coils, magnetic susceptibility artifact can be reduced. Perfluorocarbon decreases magnetic field inhomogeneity causes by mismatch of magnetic susceptibility at the air-tissue interface associated with traditional air-filled endorectal coil (29).

The ADC values of recurrent cancer in our study were similar to those values seen in foci of cancer that have not yet undergone treatment (14,20). The ADC values measured in areas of post treatment atrophy, though, appeared to be slightly lower than those seen in the untreated gland (19,20). Our results were very similar to those described in two other studies that also investigated patients with prostate cancer after radiation therapy. Sato et al. described the ADC values of cancer before (1.0×10^{-3} mm^2/s) and after successful therapy (1.6×10^{-3} mm^2/s) (20). Kim et al. described the ADC values of proven recurrence after therapy (0.98×10^{-3} mm^2/s) and of areas without recurrent disease (1.6×10^{-3} mm^2/s) (10). The reason for decreased ADC values in recurrent prostate cancer is still not entirely understood, but similar to other type of cancers, it has been speculated that increased tightly packed cells restrict diffusion of water. Whereas, the radiated atrophic prostate tissue, contains less cells to restrict water diffusion resulting in higher ADC values. These characteristics possibly make diffusion-weighted MR imaging a fairly sensitive and specific method for the detection of local recurrence.

To our knowledge, there is only one study available in the literature that looked at functional 3-Tesla MR imaging for the evaluation of suspected locally recurrent prostate cancer after external beam radiation. As in our study, Kim et al., investigating 3-Tesla diffusion-weighted MR imaging in 36 patients, but without an endorectal coil, found that the combination of diffusion-weighted MR imaging with T2-weighted MR imaging led to an improvement in the area under the ROC curve from 0.61 to 0.88 (10). These results are comparable to ours.

A few other authors have studied 1.5-Tesla MR imaging in this same group of patients. Westphalen et al. found that T2-weighted MR imaging alone has low accuracy for the detection of local recurrence (28) and that combining MR spectroscopic imaging with T2-weighted MR imaging significantly increases the area under the ROC curve, from 0.67 to 0.79 (12). The results of our study corroborate these findings. T2-weighted MR imaging, MR spectroscopic and diffusion-weighted MR imaging are not the only techniques available to evaluate patients with suspected local recurrent disease. Both Haider et al. and Rouviere et al. found that dynamic contrast-enhanced MR imaging is more accurate than T2-weighted

imaging, in particular because of greater sensitivity (9,30). More recently, Akin et al. demonstrated that the combination of both diffusion-weighted MR imaging and dynamic contrast-enhanced MR imaging with T2-weighted MR imaging improved the detection of recurrent disease. For one reader the area under the ROC increased from 64% to 95%, while for the other one it increased from 53% to 86% (31). Unfortunately, patients in this cohort did not undergo dynamic contrast-enhanced MR imaging. To our knowledge, research investigating the combination of all four MR techniques in this clinical scenario has not been published.

To date there is no consensus on how multiple MR imaging parameters should be evaluated. Some may argue that the ideal approach would be to measure ADC values and metabolic ratios of suspicious areas visualized on T2-weighted images, while others may say, for example, that ADC values should be measured at the focal area with lower signal on ADC maps, irrespective of abnormalities on the other sequences. Both approaches are valid, but answer different questions. The first one allows the reader to assess how diffusion-weighted MR imaging and MR spectroscopic imaging further characterize abnormalities seen on T2-weighted images. The second method will only characterize abnormalities identified on diffusion-weighted MR images and not take into account other imaging information. Our goal was to determine what is the best combination of information obtained from T2-weighted MR imaging, diffusion-weighted MR imaging, and MR spectroscopic imaging to detect locally recurrent prostate cancer. Although MR spectroscopic imaging alone may suffice, a trend towards improved discrimination of patients with and without disease with the combination of all three MR modalities suggests that this should be the preferable approach. Our study does not allow one to determine the order in which these images should be analyzed, nor how positive and negative results should be combined. This is a topic for additional research.

Evaluating recurrence after radiation therapy is challenging due to radiation induced fibrosis and atrophy of the prostate gland. TRUS biopsy is routinely performed despite being a invasive method fraught with sampling error (5,6,25). MRI offers a non-invasive alternative in evaluation of recurrent disease. MRI can be used clinically to identify recurrent disease and to subsequently guide a targeted biopsy if needed. Another advantage of MRI is its ability to noninvasively evaluate extracapsular disease and seminal vesicle spread. For instance, in patients with biochemical recurrence being considered for salvage prostatectomy, MRI findings of seminal vesicle invasion or extra prostatic extension will alter patient management.

Our study has limitations. First, this was a single hospital study and because acquisition expertise and equipment brand vary, our results may not be generalizable to all institutions. Second, our small sample size resulted in wide 95% confidence intervals. Our goal was not to determine the exact accuracy of each diagnostic approach, but rather to compare the performance of different MR sequence combinations. Because of these wide 95% confidence intervals, only large differences between the diagnostic performances of two different combinations of MR techniques can be demonstrated. The use of sextant biopsy results as a standard of reference may be criticized, but this approach is aligned to clinical practice. Even when local recurrence is detected, these patients seldom undergo salvage prostatectomy. In addition, the option for using prostatectomy specimens as the standard of reference would also be prone to bias, as only patients with a positive biopsy would be included in the analysis. Third, it is conceivable that patients whose post treatment MR imaging had negative results did not proceed to biopsy and therefore were not included in the study. One would expect this to have occurred more commonly for patients who ultimately do not have disease, as other clinical information would weigh in the decision to proceed to get a biopsy, irrespective of negative imaging results. This bias would lead to

results that would spuriously increase the sensitivity and decrease the specificity of MR imaging techniques. Yet, this bias would affect all MR techniques similarly and our goal was not to calculate the accuracy of MR imaging techniques, but to determine if there is an incremental value of combining them.

In conclusion, incorporation of MR spectroscopic imaging to T2-weighted MR imaging and/or diffusion-weighted MR imaging significantly improves the assessment of patients with suspected local recurrence after radiation therapy and a combined approach with all three modalities may have the best diagnostic performance.

Acknowledgments

Grant support

ACW supported by RSNA Research & Education Foundation 2007–2009 Research Scholar Grant #RSCH0709 and NIH/NCRR/OD UCSF-CTSI Grant Number KL2 RR024130. Contents are solely the responsibility of the authors and do not necessarily represent the official views of the NIH or of the Radiological Society of North America. These are career development awards without any direct role in design and conduct of the study; collection, management, analysis, and interpretation of the data; and preparation, review, or approval of the manuscript. This work was also supported by NIH grants R01CA059897 and R01CA111291 (DBV).

REFERENCES

1. American Cancer Society. Cancer Facts and Figures 2011. Atlanta: American Cancer Society; 2011. p. 19-20.
2. Cooperberg M, Broering J, Carroll P. Time trends and local variation in primary treatment of localized prostate cancer. Journal of Clinical Oncology. 2010; 28(7):1117. [PubMed: 20124165]
3. Kuban DA, Thames HD, Levy LB, et al. Long-term multi-institutional analysis of stage T1-T2 prostate cancer treated with radiotherapy in the PSA era. Int J Radiat Oncol Biol Phys. 2003; 57(4): 915–928. [PubMed: 14575822]
4. Horwitz EM, Bae K, Hanks GE, et al. Ten-year follow-up of radiation therapy oncology group protocol 92-02: a phase III trial of the duration of elective androgen deprivation in locally advanced prostate cancer. J Clin Oncol. 2008; 26(15):2497–2504. [PubMed: 18413638]
5. Roehl KA, Antenor JA, Catalona WJ. Serial biopsy results in prostate cancer screening study. J Urol. 2002; 167(6):2435–2439. [PubMed: 11992052]
6. Stewart CS, Leibovich BC, Weaver AL, Lieber MM. Prostate cancer diagnosis using a saturation needle biopsy technique after previous negative sextant biopsies. J Urol. 2001; 166(1):86–91. discussion 91-82. [PubMed: 11435830]
7. Chan TW, Kressel HY. Prostate and seminal vesicles after irradiation: MR appearance. J Magn Reson Imaging. 1991; 1(5):503–511. [PubMed: 1790374]
8. Sugimura K, Carrington BM, Quivey JM, Hricak H. Postirradiation changes in the pelvis: assessment with MR imaging. Radiology. 1990; 175(3):805–813. [PubMed: 2343132]
9. Haider MA, Chung P, Sweet J, et al. Dynamic contrast-enhanced magnetic resonance imaging for localization of recurrent prostate cancer after external beam radiotherapy. Int J Radiat Oncol Biol Phys. 2008; 70(2):425–430. [PubMed: 17881141]
10. Kim CK, Park BK, Lee HM. Prediction of locally recurrent prostate cancer after radiation therapy: incremental value of 3T diffusion-weighted MRI. J Magn Reson Imaging. 2009; 29(2):391–397. [PubMed: 19161194]
11. Pucar D, Shukla-Dave A, Hricak H, et al. Prostate cancer: correlation of MR imaging and MR spectroscopy with pathologic findings after radiation therapy-initial experience. Radiology. 2005; 236(2):545–553. [PubMed: 15972335]
12. Westphalen AC, Coakley FV, Roach M 3rd, McCulloch CE, Kurhanewicz J. Locally recurrent prostate cancer after external beam radiation therapy: diagnostic performance of 1.5-T endorectal MR imaging and MR spectroscopic imaging for detection. Radiology. 2010; 256(2):485–492. [PubMed: 20551184]

13. Choi JY, Kim MJ, Chung YE, et al. Abdominal applications of 3.0-T MR imaging: comparative review versus a 1.5-T system. Radiographics. 2008; 28(4):e30. [PubMed: 18426969]
14. Song I, Kim CK, Park BK, Park W. Assessment of response to radiotherapy for prostate cancer: value of diffusion-weighted MRI at 3 T. AJR Am J Roentgenol. 2010; 194(6):W477–W482. [PubMed: 20489065]
15. Roach M 3rd, Hanks G, Thames H Jr, et al. Defining biochemical failure following radiotherapy with or without hormonal therapy in men with clinically localized prostate cancer: recommendations of the RTOG-ASTRO Phoenix Consensus Conference. Int J Radiat Oncol Biol Phys. 2006; 65(4):965–974. [PubMed: 16798415]
16. Chen AP, Cunningham CH, Kurhanewicz J, et al. High-resolution 3D MR spectroscopic imaging of the prostate at 3 T with the MLEV-PRESS sequence. Magnetic Resonance Imaging. 2006; 24(7):825–832. [PubMed: 16916699]
17. Langer DL, van der Kwast TH, Evans AJ, Trachtenberg J, Wilson BC, Haider MA. Prostate cancer detection with multi-parametric MRI: logistic regression analysis of quantitative T2, diffusion-weighted imaging, and dynamic contrast-enhanced MRI. J Magn Reson Imaging. 2009; 30(2): 327–334. [PubMed: 19629981]
18. deSouza NM, Riches SF, Vanas NJ, et al. Diffusion-weighted magnetic resonance imaging: a potential non-invasive marker of tumour aggressiveness in localized prostate cancer. Clin Radiol. 2008; 63(7):774–782. [PubMed: 18555035]
19. Pickles MD, Gibbs P, Sreenivas M, Turnbull LW. Diffusion-weighted imaging of normal and malignant prostate tissue at 3.0T. J Magn Reson Imaging. 2006; 23(2):130–134. [PubMed: 16374882]
20. Sato C, Naganawa S, Nakamura T, et al. Differentiation of noncancerous tissue and cancer lesions by apparent diffusion coefficient values in transition and peripheral zones of the prostate. J Magn Reson Imaging. 2005; 21(3):258–262. [PubMed: 15723379]
21. Pickett B, Kurhanewicz J, Weinberg V, Pouliot J, Shinohara K, Roach M. Magnetic Resonance Spectroscopy Imaging and PSA Responses Following Three-Dimensional Conformal External Beam Radiotherapy (3DCRT) or 3DCRT plus Permanent Prostate Implant (PPI) for Intermediate Risk Prostate Cancer. International Journal of Radiation Oncology*Biology*Physics. 2005; 63(Supplement 1):S142–S172.
22. Pickett B, Ten Haken RK, Kurhanewicz J, et al. Time to metabolic atrophy after permanent prostate seed implantation based on magnetic resonance spectroscopic imaging. International Journal of Radiation Oncology*Biology*Physics. 2004; 59(3):665–673.
23. Roach M 3rd, Kurhanewicz J, Carroll P. Spectroscopy in prostate cancer: hope or hype? Oncology (Williston Park). 2001; 15(11):1399–1410. discussion 1415-1396, 1418. [PubMed: 11758871]
24. Kestin LL, Goldstein NS, Vicini FA, et al. Pathologic evidence of dose-response and dose-volume relationships for prostate cancer treated with combined external beam radiotherapy and high-dose-rate brachytherapy. Int J Radiat Oncol Biol Phys. 2002; 54(1):107–118. [PubMed: 12182980]
25. Crook J, Malone S, Perry G, Bahadur Y, Robertson S, Abdolell M. Postradiotherapy prostate biopsies: what do they really mean? Results for 498 patients. Int J Radiat Oncol Biol Phys. 2000; 48(2):355–367. [PubMed: 10974448]
26. Liang KY, Zeger SL. Longitudinal data analysis using generalized linear models. Biometrika. 1986; 73:13–22.
27. Davison, A.; Hinkley, D. Bootstrap Methods and Their Application, Cambridge Series in Statistical and Probabilistic Mathematics. Cambridge: Cambridge University Press; 1997. Confidence Intervals; p. 191-251.
28. Westphalen AC, Kurhanewicz J, Cunha RM, et al. T2-Weighted endorectal magnetic resonance imaging of prostate cancer after external beam radiation therapy. Int Braz J Urol. 2009; 35(2):171–180. discussion 181-172. [PubMed: 19409121]
29. Noworolski SM, Crane JC, Vigneron DB, Kurhanewicz J. A clinical comparison of rigid and inflatable endorectal-coil probes for MRI and 3D MR spectroscopic imaging (MRSI) of the prostate. J Magn Reson Imaging. 2008; 27(5):1077–1082. [PubMed: 18407539]

30. Rouviere O, Valette O, Grivolat S, et al. Recurrent prostate cancer after external beam radiotherapy: value of contrast-enhanced dynamic MRI in localizing intraprostatic tumor--correlation with biopsy findings. Urology. 2004; 63(5):922–927. [PubMed: 15134982]

31. Akin O, Gultekin DH, Vargas HA, et al. Incremental value of diffusion weighted and dynamic contrast enhanced MRI in the detection of locally recurrent prostate cancer after radiation treatment: preliminary results. Eur Radiol. 2011; 21(9):1970–1978. [PubMed: 21533634]

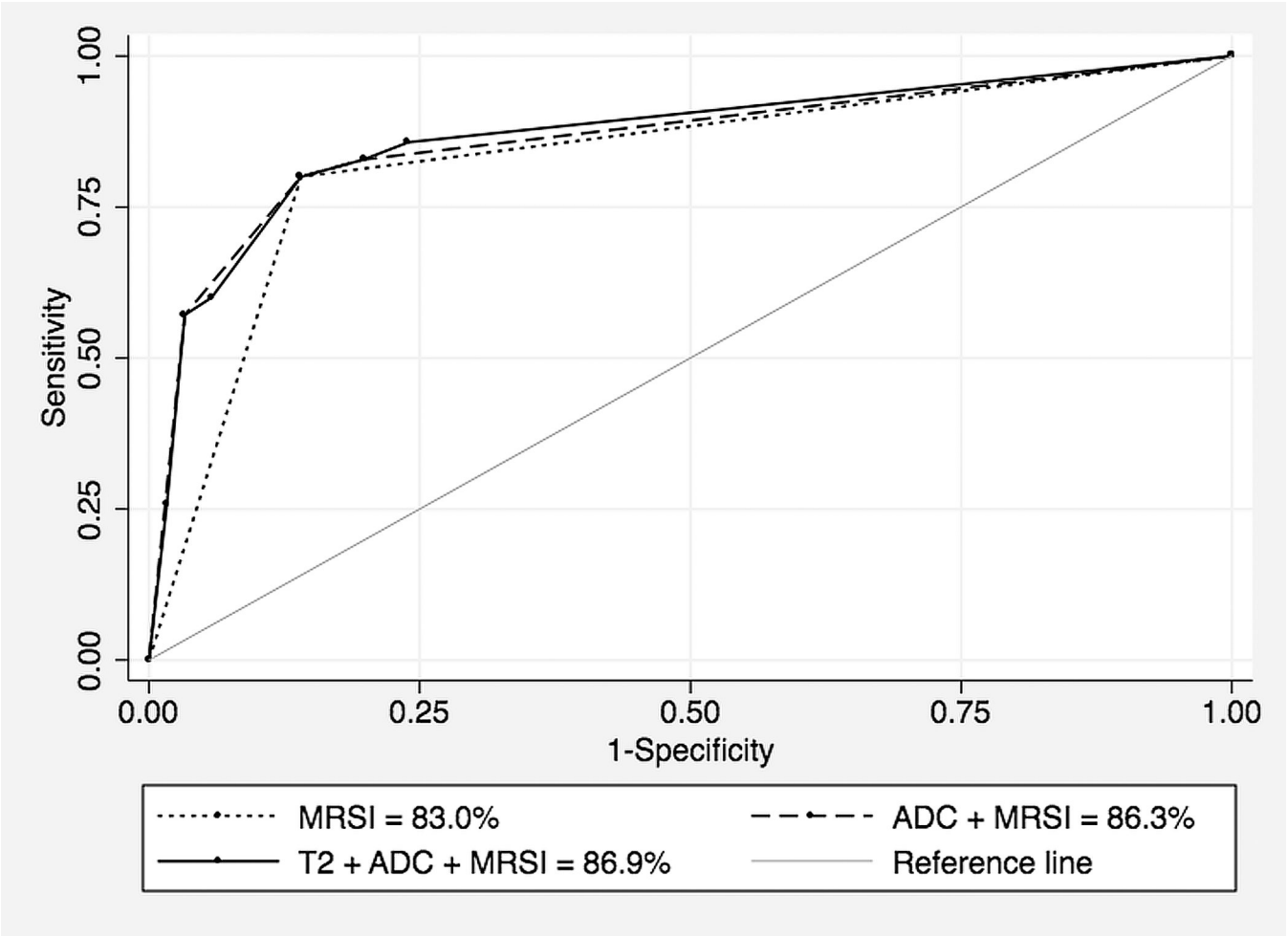

Figure 1.

Receiver operating characteristic curves for detection of locally recurrent prostate cancer after external beam radiation therapy with MR spectroscopic imaging (dotted line), combined diffusion-weighted MR imaging and MR spectroscopic imaging (dashed line), and combined T2-weighted MR imaging, diffusion-weighted MR imaging, and MR spectroscopic imaging (thick solid line). Lower thin solid line is reference line.

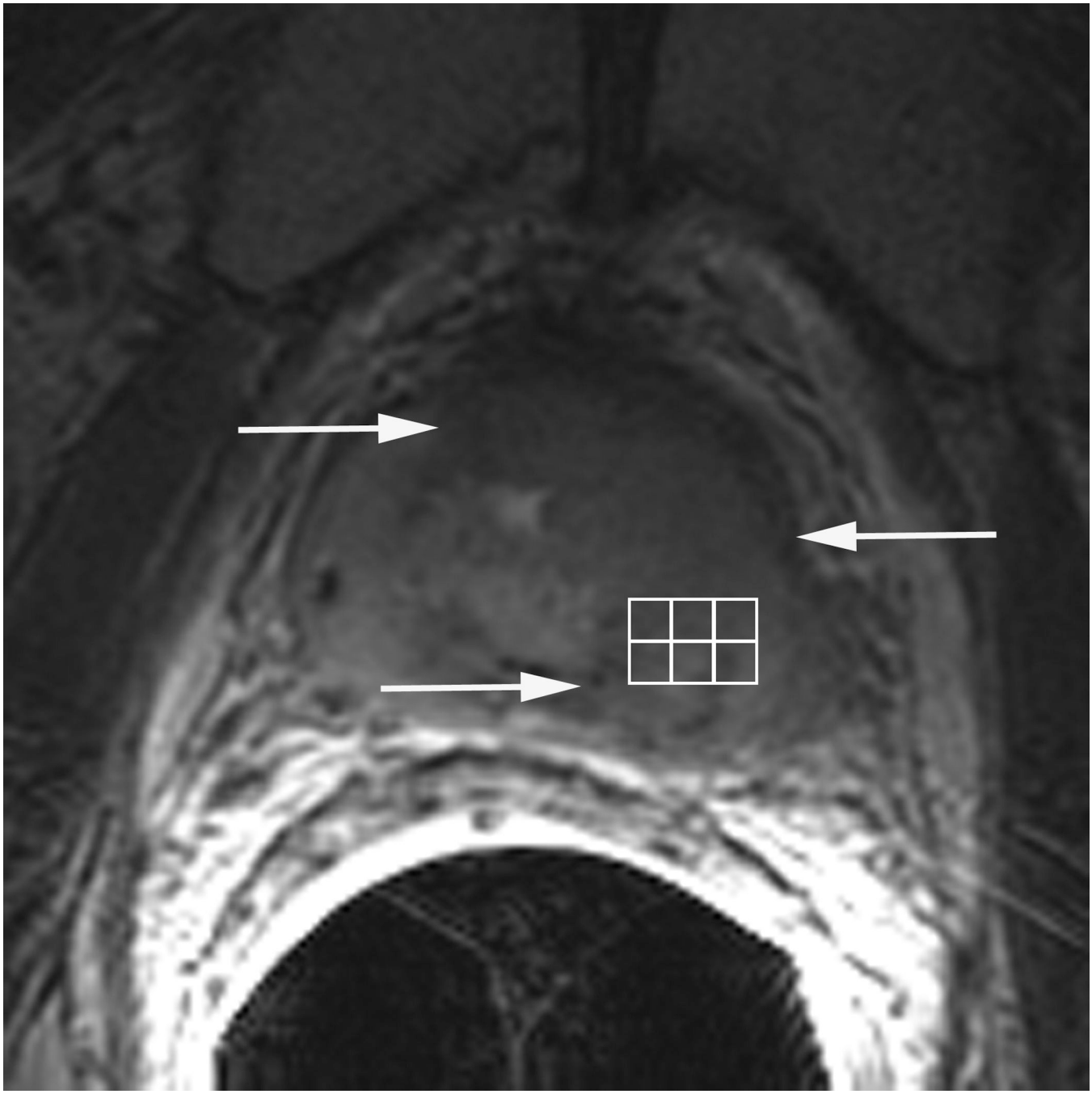

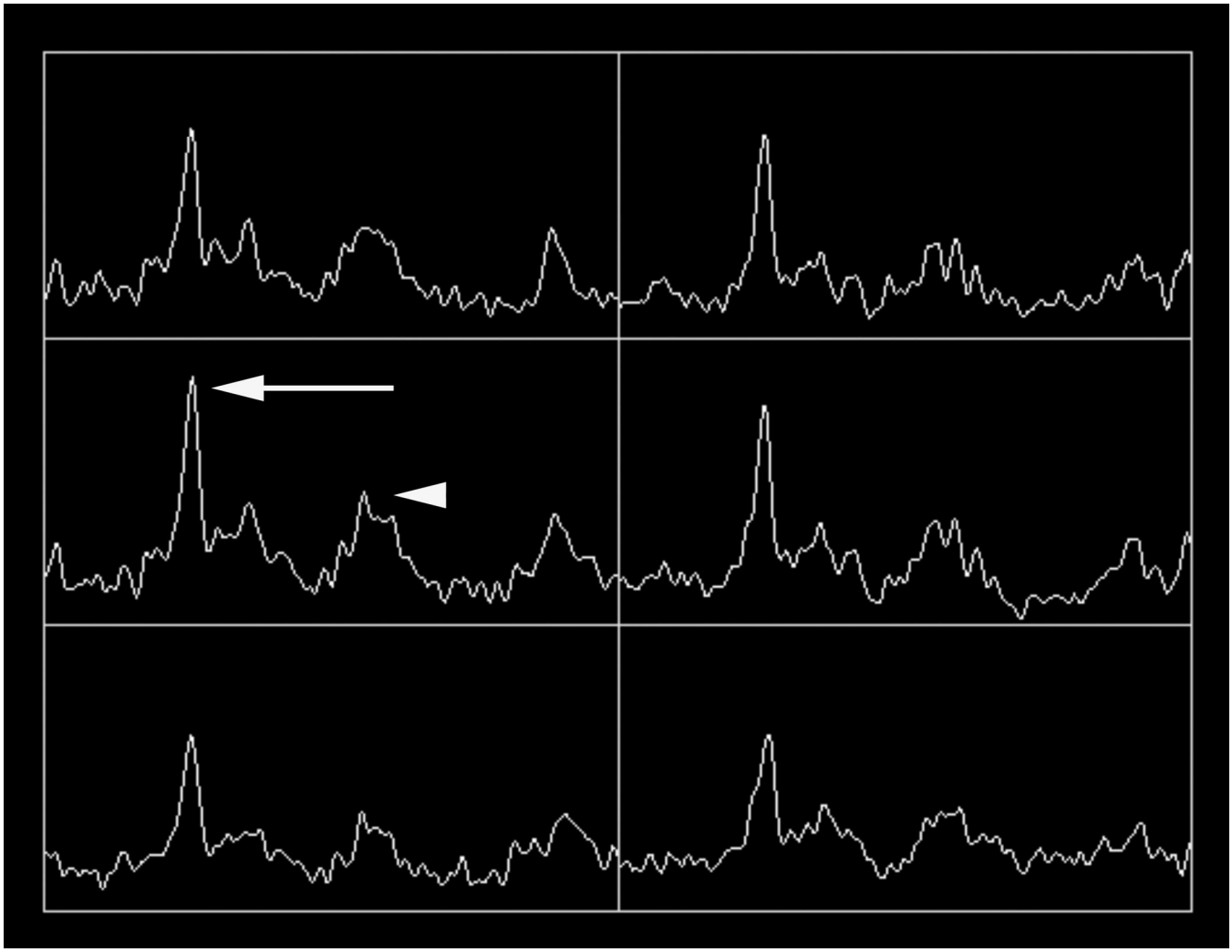

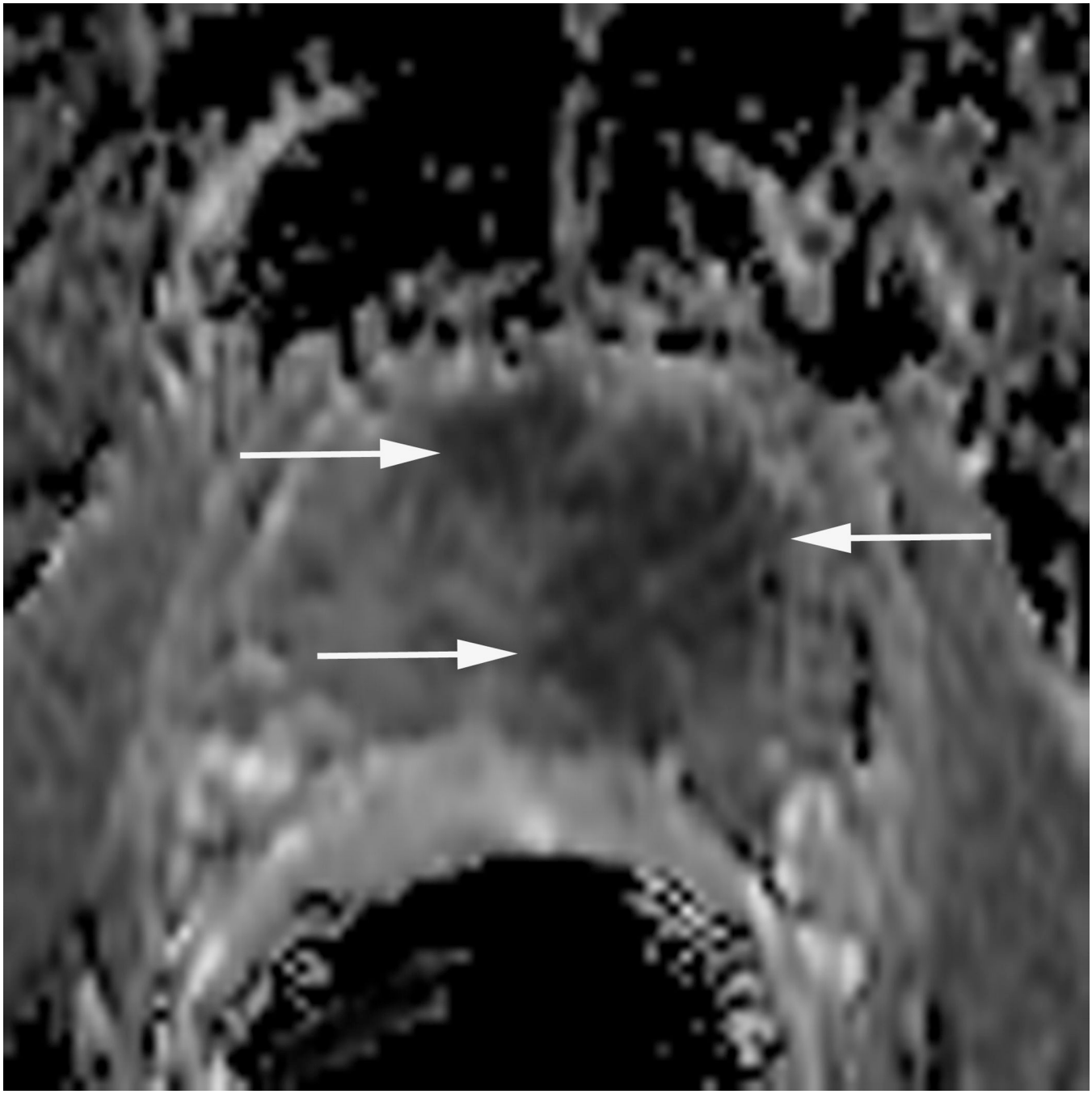

Figure 2.
77 year-old man with biopsy proven recurrent prostate cancer in the left gland. T2-weighted MR image demonstrates a large focal area of decreased signal intensity, consistent with recurrent cancer (arrows in A). Grid (in A) with corresponding MR spectra showing high choline (arrow in B) and low citrate peaks (arrowhead in B), characterizing malignant metabolism. ADC map demonstrates restricted diffusion in the same area (arrows in C).

Table 1

Areas under the ROC curves for the detection of recurrent disease after radiation therapy with T2-weighted MR imaging, diffusion-weighted MR imaging, and MR spectroscopic imaging, alone or in combination.

Techniques	Az	95% confidence interval
T2	0.616	0.511 to 0.732
ADC	0.755	0.610 to 0.853
MRSI	0.830	0.755 to 0.891
T2 + ADC	0.774	0.604 to 0.869
T2 + MRSI	0.841	0.765 to 0.909
ADC + MRSI	0.863	0.775 to 0.933
T2 + ADC + MRSI	0.869	0.776 to 0.934

T2 = T2-weighted MR imaging
ADC = apparent diffusion coefficient
MRSI = MR spectroscopic imaging
Az = area under the receiver operating characteristic curve

Table 2

Differences between areas under the ROC curves for the detection of local recurrence obtained comparing single MR imaging techniques and all possible combinations.

Techniques	*P* value	Difference	95% confidence interval
T2 versus ADC	0.07	−13.9	−28.4 to 0.2
T2 versus MRSI	<0.001	−21.4	−34.7 to −9.0
T2 versus T2 + ADC	0.03	−15.8	−29.5 to −2.5
T2 versus T2 + MRSI	<0.001	−22.5	−35.7 to −12.4
T2 versus ADC + MRSI	<0.001	−24.7	−38.9 to −12.7
T2 versus T2 + ADC + MRSI	<0.001	−25.3	−39.4 to −13.9
ADC versus T2	0.07	13.9	−0.2 to 28.4
ADC versus MRSI	0.20	−7.5	−21.1 to 1.6
ADC versus ADC + T2	0.33	−1.9	−6.9 to 0.7
ADC versus ADC + MRSI	0.02	−10.8	−24.0 to −4.9
ADC versus T2 + MRSI	0.15	−8.6	−21.3 to 0.8
ADC versus ADC + T2 + MRSI	0.02	−11.4	−24.5 to −5.3
MRSI versus T2	<0.001	21.4	9.0 to 34.7
MRSI versus ADC	0.20	7.5	−1.6 to 21.1
MRSI versus MRSI + T2	0.41	−1.1	−4.3 to 1.2
MRSI versus MRSI + ADC	0.13	−3.3	−7.7 to 1.0
MRSI versus T2 + ADC	0.38	5.6	−4.4 to 19.8
MRSI versus MRSI + T2 + ADC	0.09	−3.9	−8.4 to 8.3
T2 + ADC versus T2 + MRSI	0.27	−6.7	−19.9 to 2.8
T2 + ADC versus ADC + MRSI	0.03	−8.9	−23.0 to −1.2
T2 + MRSI versus ADC + MRSI	0.40	−2.2	−7.2 to 2.6
T2 + ADC versus T2 + ADC + MRSI	0.04	−9.5	−22.3 to −3.1
T2 + MRSI versus T2 + ADC + MRSI	0.18	−2.8	−7.5 to 0.6
ADC + MRSI versus T2 + ADC + MRSI	0.65	−0.6	−3.3 to 1.6

T2 = T2-weighted MR imaging, ADC = apparent diffusion coefficient, MRSI = MR spectroscopic imaging